Measurement 189 (2022) 110458

Contents lists available at ScienceDirect

Measurement

journal homepage: www.elsevier.com/locate/measurement

Compressible gas density measurement by means of Fourier analysis of interferograms

Janusz Telega [a,*], Ryszard Szwaba [a], Małgorzata A. Śmiałek [b]

[a] Institute of Fluid Flow Machinery, Polish Academy of Sciences, Fiszera 14, 80-231 Gdansk, Poland
[b] Institute of Naval Architecture and Ocean Engineering, Faculty of Mechanical Engineering and Ship Technology, Gdansk University of Technology, Narutowicza 11/12, 80-233 Gdańsk, Poland

ARTICLE INFO

Keywords:
Density measurement
Fourier image analysis
Interferometry
Shock wave

ABSTRACT

This paper describes a method for nonintrusive compressible gas density measurement by means of automated analysis of interferograms using FFT (Fast Fourier Transform), and its implementation using DFT (Discrete Fourier Transform), that does make this measurement technique a fairly valuable and accessible experimental method. The presented approach makes it possible to use the finite fringe setting of the interferometer, thus reducing adjustment time. In the process of analysis, the errors originating from the imperfections of optical elements are reduced, and a digital image of a virtual infinite setting of the instrument is generated. As described here, the method is extremely beneficial, but not limited to, flows with shock wave – boundary layer interactions. A result of density measured for a flow with shock wave is presented.

1. Introduction

Optical interferometry used to be a widely exploited measurement technique for compressible fluid flow research. It is suitable for applications involving flows with shock waves, and any other flow structures inducing strong density gradients. A popular optical setup for obtaining interferograms is a Mach-Zender interferometer [1].

Depending on the adjustment of the interferometer, it can be used in the infinite fringe mode or in the finite fringe mode [2]. The infinite fringe mode requires positioning both mirrors so that they are parallel. The results are easy to interpret, but the actual adjusting of the interferometer is very time-consuming in this mode [3]. In specific fields like investigation of the topology of shock wave [4] this semi – quantitative result is sufficient.

The finite fringe mode adjustment reduces the adjustment time and can be used with lower quality optical components. The analyzing of results in this mode requires two interferograms (with flow and without flow) to find the points of intersection of corresponding fringes, allowing one to calculate the density differences.

The above approaches are very inefficient in terms of using the information contained in the interferogram. They reduce the range of phase values to a single bit. This takes place, as the fringe distribution in the plane is replaced by contours and the image is reduced to a binary one.

A much more efficient method is based on Fourier transform [5,6], described in this paper. After being first published, the method of decoding information from fringe pattern has been a subject to intensive studies to improve the performance of it [7] A review of the cutting-edge applications of the method are described in [8]. A method of discarding the constant component using two fringe patterns shifted by angle of π was proposed in [9]. An inevitable problem of frequency leakage and the performance of windowing functions in reducing it was investigated in [10].

The important part of the method is phase unwrapping. The algorithms for doing it can be classified into local path dependent or path-following ones and global (path-independent) approaches. Local algorithms, like Goldstein path-following method (published in 1988), D.J. Bone second difference method (published in 1991), Flynn's minimum weighted discontinuity method (published in 1997), algorithm based on FFT sorting by reliability following a non-continuous path (published in 2002) use pixel-to-pixel integration and thus rely on the local values of wrapped phase along a chosen path. Global or path-independent methods attempt to minimize the difference between the gradients of the wrapped and the gradients of the unwrapped solution in both × and y directions. A novel approach for aiding phase unwrapping in the presence of discontinuities called 'multi-channel Fourier fringe analysis'

* Corresponding author.
E-mail addresses: januszt@imp.gda.pl (J. Telega), rssz@imp.gda.pl (R. Szwaba), smialek@pg.edu.pl (M.A. Śmiałek).

https://doi.org/10.1016/j.measurement.2021.110458
Received 11 August 2021; Received in revised form 28 October 2021; Accepted 9 November 2021
Available online 14 November 2021

is proposed in [11]. It is based on the invariance of discontiunuities against varying angle or frequency. An extensive review of the 'classic; fringe pattern analysis can be found in [12]. A very modern approach to solving the problems generated by the Fourier analysis approach can be found in [13], where authors present their work on machine learning using deep neural network to increase the amount of information that can be obtained from a given amount of fringe pattern.

The paper illustrates the very good applicability of the FTFA method for the experiments in the field of flows with shock waves. The presented implementation is relatively simple, as compared against holography method, yet still the results are proven to be in a very good agreement to more 'classical' methods. The possibility of using the method for analysis of shape of shock wave and the temporal evolution of it as well as the ability to do the measurements in a very sensitive zone of triple point, that is new and a very desired in this field is described. An assessment of the error resulting from the real distribution of the laser light source is also given.

2. Method

The method of analysis is well suited for any phenomenon that involves density changes of gas like combustion, but the description will be illustrated by the field of interest of authors, which concerns the supersonic flows and SWBLI (Shock Wave – Boundary Layer Interaction). For flows involving the appearance of a shock wave, a nonintrusive measurement inside the boundary layer is of great value.

The analysis exploits two interferograms of two flow conditions: a no-flow condition as in Fig. 1 a) and a flow-on condition with shock wave as in Fig. 1 b).

The measurements were carried out at the IMP PAN supersonic wind tunnel facility. The wind tunnel is an intermittent, vacuum type wind tunnel, a scheme of it is given in Fig. 2.

The tunnel is, described in more detailed manner in [14]. The test nozzle is schematically depicted in Fig. 3.

The interferogram depicts the flow in a convergent-divergent nozzle with Mach number value upstream the shock wave of 1.34. The height of the nozzle throat is approximately 100 mm and the width of the chamber is 100 mm. The measurements were conducted with inlet stagnation temperature of 297 K and inlet stagnation pressure of 101.5 kPa.

Due to some geometrical restrictions just the area indicated with red and yellow fringes in Fig. 3 is visible in interferograms. The shape of it is an intersection of the circular tunnel windows of 100 mm diameter, interferometer mirrors and the CCD chip. The interferometer setup is illustrated in Fig. 4.

The schematic of the interferometer is given in the left-hand (a) side of Fig. 4 and the right-hand side of this figure depicts the instrument that has been used in the measurements. It is built on a stone plate of shape allowing to optically cover the measurement chamber.

The camera was an 8-bit monochromatic CCD camera.

3. Theory

The method can be divided into four main stages: Fourier transformation of interferograms, extraction of region containing information, calculation of phase shift map, calculation of density map.

3.1. Fourier transformation of signals

The light intensity of a finite fringe setting in a constant density condition, in the ideal case of a uniform light source and the use of perfect optical components can be described as:

$$i(\vec{r}) = m \bullet \cos(2 \bullet \pi \bullet \vec{\nu_0} \bullet \vec{r}) \tag{1}$$

where

$i(\vec{r})$ is the intensity in the point r $\vec{}$of the observation plane,

m is the amplitude of light,

$\vec{\nu_0}$ is the heterodyning frequency introduced by the tilt of one of the mirrors.

The heterodyning frequency is a result of the optical path length that is changing linearly (for the flat mirrors that are used here) with changing the position in the image plane. This linear change gives rise to linear phase shift between the rays resulting in the sinusoidal light pattern in the image for the no-flow conditions. The spatial frequency is a function of the direction with respect to the axis of mutual tilting of the mirrors.

In applying the FTFA to actual experimental interferograms it is crucial to use values of luminosity recorded in each pixel, and not an image of luminosity mapped using the gamma-correction algorithm, which is a default for almost every modern cameras. Using the gamma-corrected images would results in errorous results, as all the analysis described is valid for the $i(\vec{r})$ being linearly proportional to the luminosity, not to the luminosity to the power of gamma ($\gamma \neq 1$).

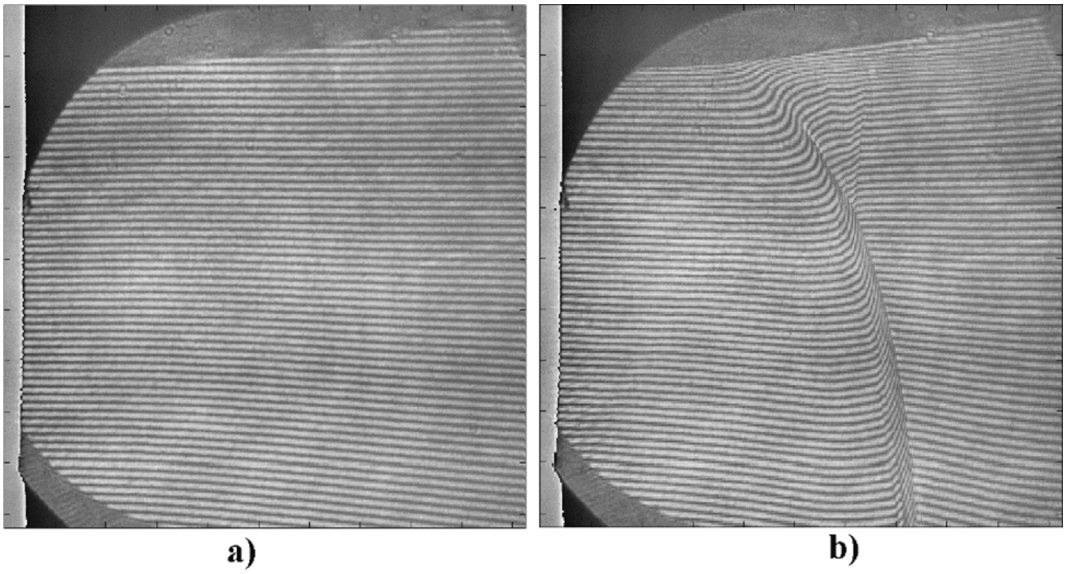

Fig. 1. No-flow (a) and flow-on (b) interfrerogram.

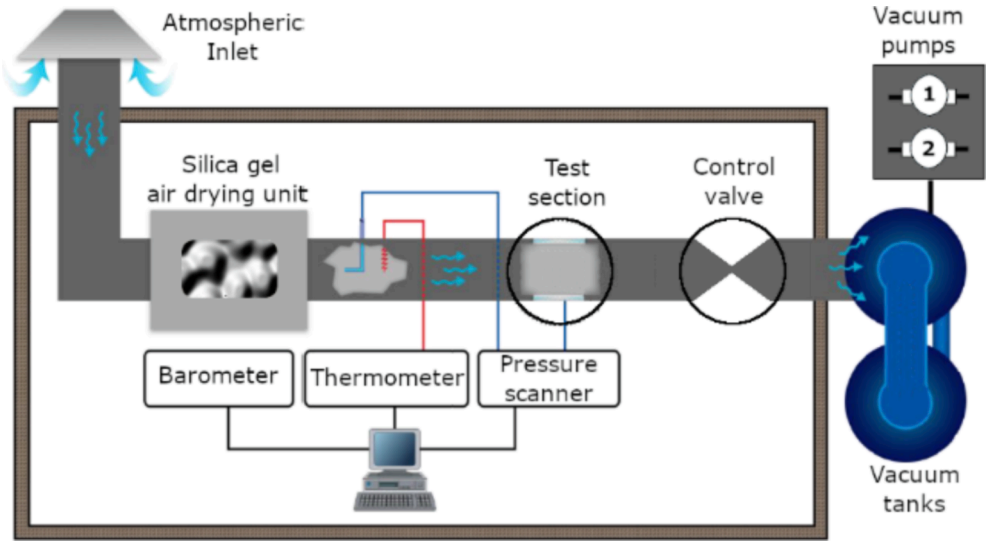

Fig. 2. Wind tunnel facility.

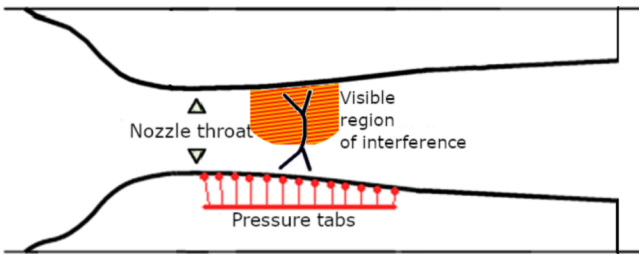

Fig. 3. Test section.

In this very specific application the heterodyning is a result of attempt to use the easier setting of interferometer and make it possible to analyze the results in a relatively easy and computationally not expensive, well known way that can be automated. Adjusting the finite fringe setting of the interferometer is easier in terms of adjustment time and as a 'side effect' it introduces a constant frequency that corresponds to carrier frequency. A significant advantage from signal processing point of view is that introducing a sufficiently high carrier frequency and heterodying gives the benefit of separating zones from each other (in the frequency domain) and still containing all the information. This approach allows one to use DFT based analysis with all of the numerical advantages of it instead of more complicated methods based on morphological analysis of interferograms. The resulting separation in the frequency domain allows us to demodulate the data from the region adjacent to the carrier frequency with good S/N ratio.

The description of data from actual experiments needs to be more complex than (1). The amplitude is modulated by a non-uniform light source, bias light and noise. The phase of the signal is modified by the flow, which is beneficial as provides all the useful information, and by imperfections of the optical system. Taking this into account, the distribution of intensity can be described by equation (2):

$$i(\vec{r}) = m(\vec{r}) \cdot cos(2 \cdot \pi \cdot \vec{\nu_0} \cdot \vec{r} + \phi(\vec{r})) + h(\vec{r}) \cdot \cos(2 \cdot 2 \cdot \pi \cdot \vec{\nu_0} \cdot \vec{r} + \phi(\vec{r})) + b(\vec{r}) \cdot + n(\vec{r}), \quad (2)$$

where•

$m(\vec{r})$•is the low frequency modulation of a real light source,

$\phi(\vec{r})$ is the phase shift,

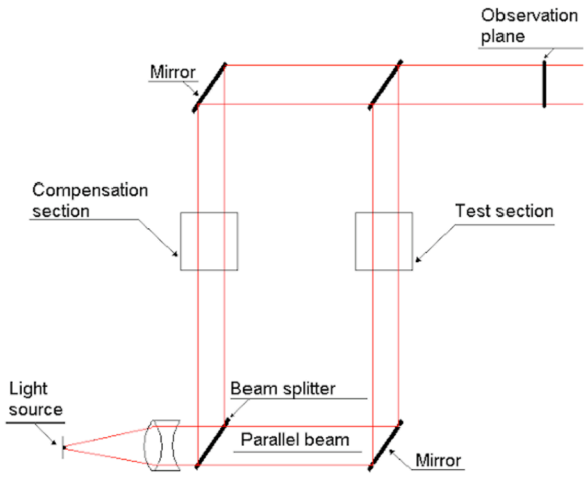

a)

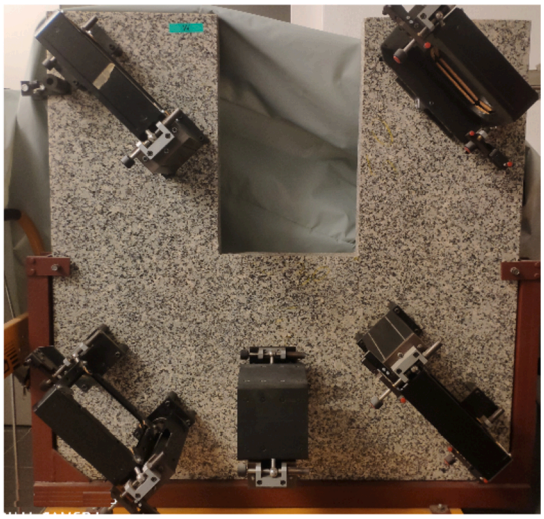

b)

Fig. 4. Interferometer schematic (a) and actual layout (b).

$h(\vec{r})\bullet$is the modulation of the first overtone,

$b(\vec{r})$ is the bias light,

$n(\vec{r})$ is the noise.

As described above, phase shift $\phi(\vec{r})$ is a sum of two components:

$\phi(\vec{r}) = \phi_0(\vec{r}) + \phi_1(\vec{r})$, where

$\phi_0(\vec{r})$ is the flow signal,

$\phi_1(\vec{r})$ is the signal induced by optical imperfections of the instrument.

To calculate the phase, the light intensity signal is transformed from space domain to frequency domain. In order to do this, a Fourier transform of the signal is calculated. The transform of the ideal, theoretical signal (1) yields:

$I(\vec{v}) = \int_r i(\vec{r})\bullet \exp(-2\bullet\pi\bullet j\bullet \vec{v}\bullet \vec{r})\bullet dr$, where

$I(\vec{v})$ is the transform of the brightness of the recorded PIXEL signal (in the frequency domain).

Calculating the intensity of the ideal signal yields:

$I(\vec{v}) = \frac{1}{2}\bullet(\delta(\vec{v} - \vec{v_0}) + \delta(\vec{v} + \vec{v_0}))$, where (2)

δ is the Dirac Delta.

By calculating the Fourier transform of signal (2) one obtains:

$I(\vec{v}) = \frac{1}{2} * M * Q(\vec{v} - \vec{v_0}) + \frac{1}{2} * M * Q(-\vec{v} - \vec{v_0}) +$ (3)

$$\frac{1}{2} * H * Q * Q(\vec{v} - 2\bullet\vec{v_0}) + \frac{1}{2}\bullet H * Q * Q(-\vec{v} - 2\bullet\vec{v_0}) + B(\vec{v}) + N(\vec{v}), \text{where}$$

$$Q(\vec{v} - \vec{v_0}) = F\{exp[j\bullet\phi(\vec{r})]\}$$

* is the convolution operator.

3.2. Extraction of region of interest

From equation (3) it can be seen, that various components of the signal are separated in the transform plane. This decomposition is the main reason for conducting the Fourier transform; at this stage the importance of a sufficiently high heterodyning frequency (obtained by adjusting the interferometer in the constant density condition) is clearly seen. The sufficiently high frequency value prevents the regions from overlapping and so allows the information to be extracted. After having all the components separated, one can easily distinguish and select the desired component for further analysis. The best choice is to select one of the first overtone regions (in theory the same information is also contained in regions adjacent to higher overtones, but the higher the overtone, the lower the signal-to-noise ratio). The power spectra of the transforms are also calculated for the purposes of visualisation.

Fig. 5 depicts a power spectrum of a flow-on interferogram from Fig. 1 b). In the central part, there is a peak of very low frequency components (including a constant component that corresponds to the mean intensity value of the whole image). All the subsequent images do not depict complex transforms but their power spectra, which have real, non-negative values that are convenient for visualization.

Higher overtones can be seen on both sides of the low frequency peak. As mentioned earlier, the amplitude of higher overtones decreases. If we decide to use the information from the first region around the $G(\vec{v}) = \frac{1}{2}\bullet M \otimes Q(\vec{v} - \vec{v_0})$, we have to extract it from the rest of the frequency plane. The first step is to apply the high pass filter thus removing the components resulting from light source modulation and mean light intensity, with the resulting spectrum as depicted in Fig. 6 a).

The next step is to remove the second overtone by applying a band pass filter that produces a spectrum given in Fig. 6b). Succeeding move is to remove the negative part of the plane that duplicates the information from the later part. This yields a result like in Fig. 6c). The final stage is to shift the transform in such a way that the position of first peak ($\vec{v_0}$ - component) is at the centre, thus realising the variables change from $\vec{v}$ to $\vec{v} - \vec{v_0}$, as depicted in Fig. 6 d). This means that we do not take into account the value of frequency (with respect to the zero value), but the change of frequency (with respect to heterodyning frequency).

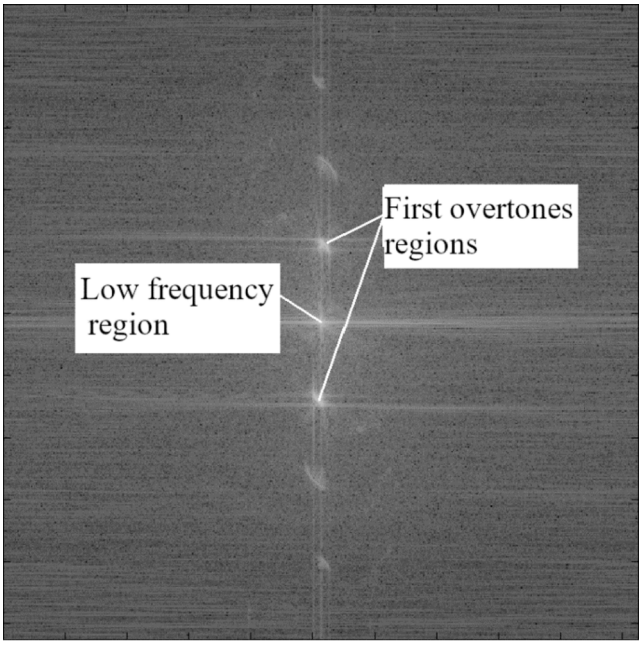

Fig. 5. Power spectrum of the image.

From this filtered and shifted data, a region representing the $G(\vec{v}) = \frac{1}{2}\bullet M \otimes Q(\vec{v} - \vec{v_0})$ can be extracted, as illustrated in Fig. 7.

3.3. Generation of phase shift map

To generate the phase map it is necessary to conduct an inverse Fourier transformation of the $G(\vec{v})$ component, obtaining $g(\vec{r}) = \frac{1}{2}\bullet m(\vec{r})\bullet\exp[j\bullet\phi(\vec{r})]$). Now the phase can be calculated using the following formula:

$$\phi(\vec{r}) = atan\left[\frac{Im[g(\vec{r})]}{Re[g(\vec{r})]}\right] \quad (4)$$

In some cases this can be a final result, but in cases involving high density gradients the overall change of phase in the flow field is bigger than π. This is almost inevitable in flows with shock waves, while formula (4) returns the phase in the range of $\langle -\frac{\pi}{2}, \frac{\pi}{2}\rangle$; the real phase value is expressed modulo π.

Hereafter a local method [15] is used.

Starting at any point of a known phase the procedure examines the magnitude of phase change when moving to an adjacent point. If this change is too large (close to π), the algorithm adds or subtracts from this value a product of π and a suitable integer value to make the change no bigger than the assumed value.

Such an approach is not sufficient for flows with shock waves and regions without light (bad pixels in the camera, side walls of the nozzle, imperfections of optical components). A shock wave can produce a change of density that is represented by a phase change bigger than π between adjacent pixels of the image. If the unwrapping algorithm meets such a point, it will unwrap it and cause an error (the information about the shock wave will be lost and this error will propagate, shifting all the values that undergo unwrapping afterwards). Also regions of underexposure or overexposure lead to low fringe contrast that can result in additional phase unwrapping errors. To avoid these problems, a masking algorithm has been applied. It is based on the value of the amplitude of an inverse Fourier transform, and masks the regions where this value is lower than a user-specified value.

A complete mask is depicted in the left hand side (a) of Fig. 8.

The right hand side (b) part of Fig. 8 depicts a result of merging an actual interferogram from Fig. 1 b) and the mask, and clearly shows that

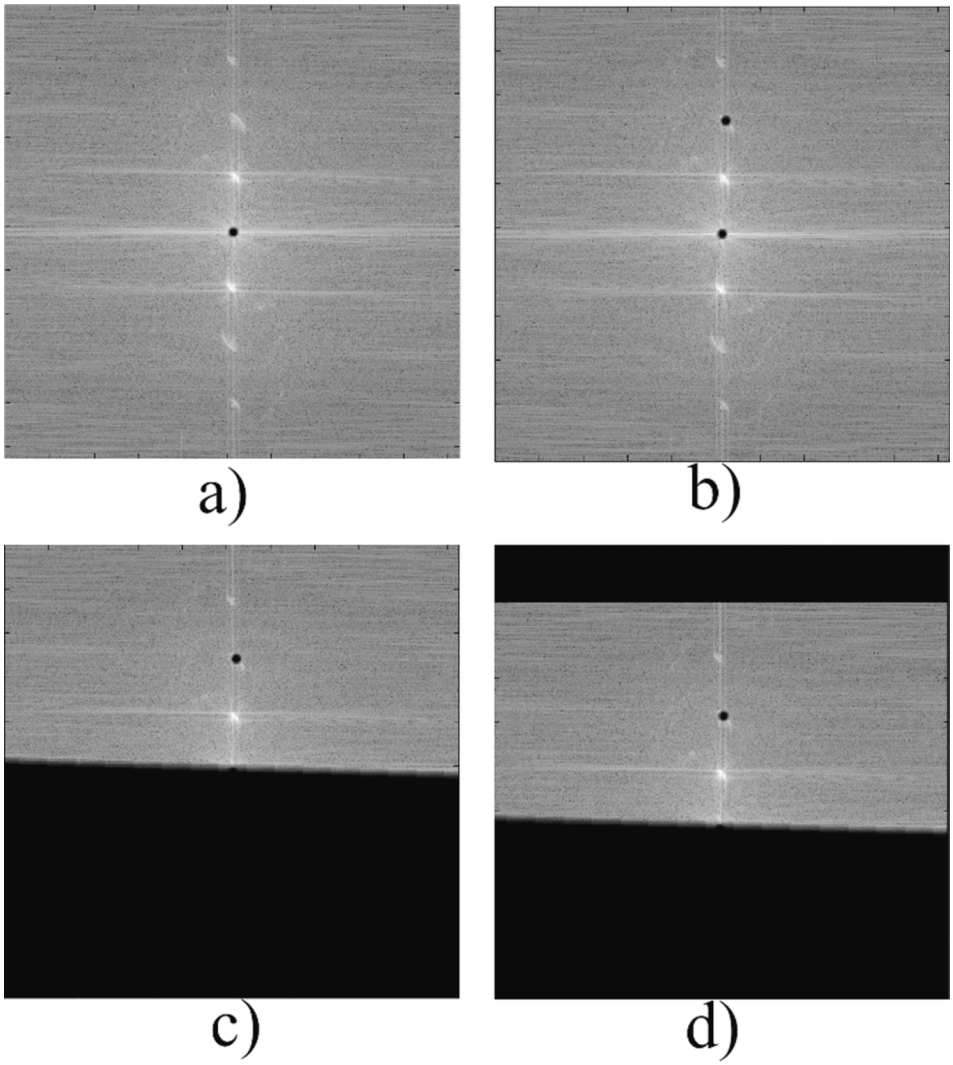

Fig. 6. Filtering in frequency domain.

the masked region corresponds directly to the position of the shock wave. In the case of such a mask, the unwrapping algorithm must be capable of finding and unwrapping all the unmasked points without using the values from masked regions. This is done by using the flood-fill algorithm. Unwrapping proceeds until the point that is to be unwrapped is masked; this point is omitted and instead the algorithm searches for an adjacent unmasked point that can be successfully unwrapped [16]. Fig. 9 depicts a possible path of the proceeding phase-unwrapping algorithm. The region of boundary layer below the shock wave marked in red colour is a region of small density gradients (causing phase change smaller than π between adjacent pixels) that is always present in an internal flow with shock wave. The presence of it is crucial for the analysis as it allows the unwrapping algorithm to proceed beyond the shock wave. Thus knowing the density value in just any single point is sufficient to calculate it also in points beyond the shock wave.

By continuing the process, a complete phase can be defined. After phase unwrapping, a phase shift map is generated by simply subtracting the phase map of the flow-on image from the map obtained after analysing the flow-off image. This removes any phases shifts caused by optical defects present in both images.

3.4. Generation of density map

The density map can be calculated by taking into account the Gladstone-Dale equation [17]:

$$\phi(x,y) = \frac{2 \bullet \pi}{\lambda} \bullet (\mathrm{n_{ref}} - \mathrm{n_{flow}(x,y)}) \bullet \mathrm{d}$$

λ is the length of light wave used,
n is the refractive index of the gas,
d is the length of the optical path inside the test section,
which is then combined with

$$n = 1 + K \bullet \rho$$

K is the Gladstone-Dale constant.

From the above formulas it is clear that density is a linear function of the phase shift. Nevertheless, it must be clearly stated, that the above is true for an assumption of two-dimensional distribution of flow parameters. If the flow parameters change as a function of the third coordinate (which is always the case, due to for example boundary layers, resulting in velocity non-uniformity across the tunnel), the obtained result is not precisely density. It is a mean value of the density (the result is being 'integrated' along the path of the ray). This is an inevitable disadvantage of all optical methods based on the travel of the light beam across the flow from very 'vintage' schlieren method [17] to relatively modern techniques like digital laser speckle photography DLSP [18,17]. Knowing the density in any point is enough to transform a phase shift map into a density map (simply by multiplying it by a proper constant value). This point can be conveniently chosen, it only has to be visible in the interferograms. For the experimental easiness, one may choose a

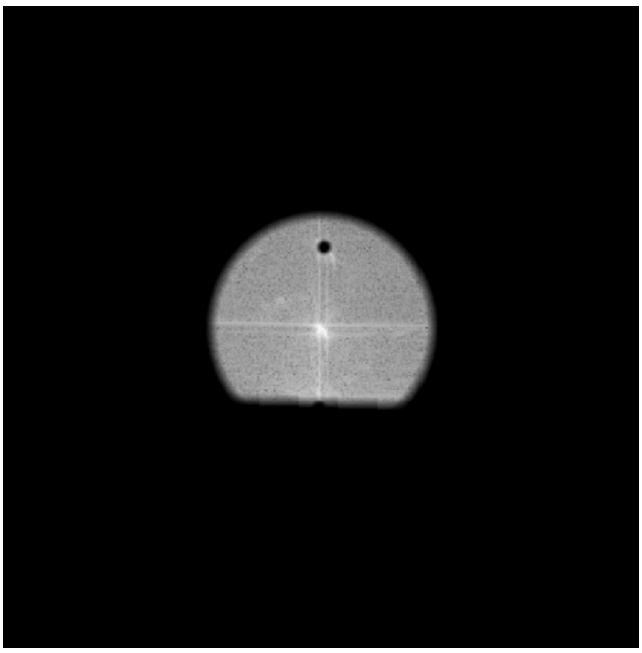

Fig. 7. Phase data in transform plane.

point sufficiently distant from the details of interest. Doing so allows one to simply place pressure and temperature probes in the flow and measure the parametres in this point, not introducing any disturbances in the region of interest. Once this is completed, other parameters of the flow can be calculated, depending on the experiment. Combining the interferometer-obtained density with the equation of state, authors of [19] resolve a temperature field in the gas flow. As it is visible from equation (5), the result is not a function of time. It means that the possible measurement frequency is limited only by camera and light source, exactly like in schlieren visualisation. Therefore in any research concerning time evolution of flow parameters like shock wave instabilities [20,21], where schlieren technique is applied it can be replaced with FTFA, giving a quantitative dimension to the qualitative schlieren results. The FTFA method can be also very successfully applied in any test stand that has been prepared to use modern LDA method, as it ensures optical access to the test volume, including subsonic flow structure research [22], or complex turbine leakage flows [23].

3.5. Uncertainty analysis

For estimation of uncertainty, it is more convenient to take into account the form of equation used by the authors of [24], following the approach of the authors of [25]:

$$\rho_{flow} - \rho_{ref} = \frac{\rho_s}{2 \bullet \pi \bullet d \bullet} \delta . \lambda . \left(\phi_{ref} - \phi_{flow} \right) \tag{5}$$

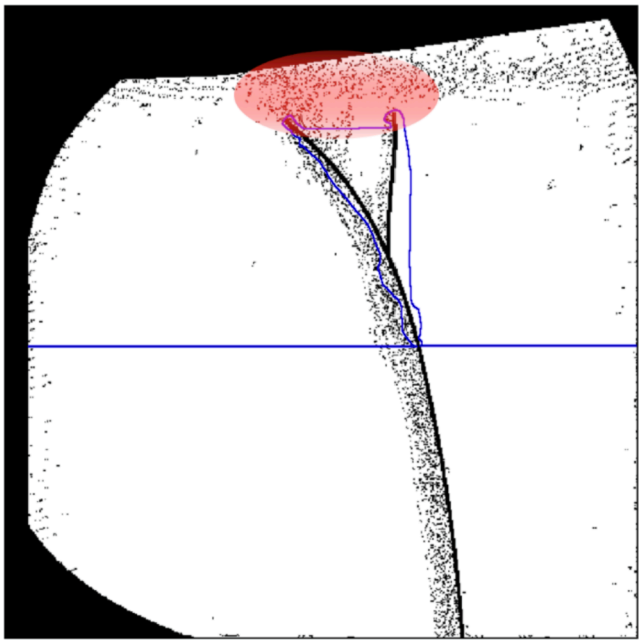

Fig. 9. Possible path of phase unwrapping.

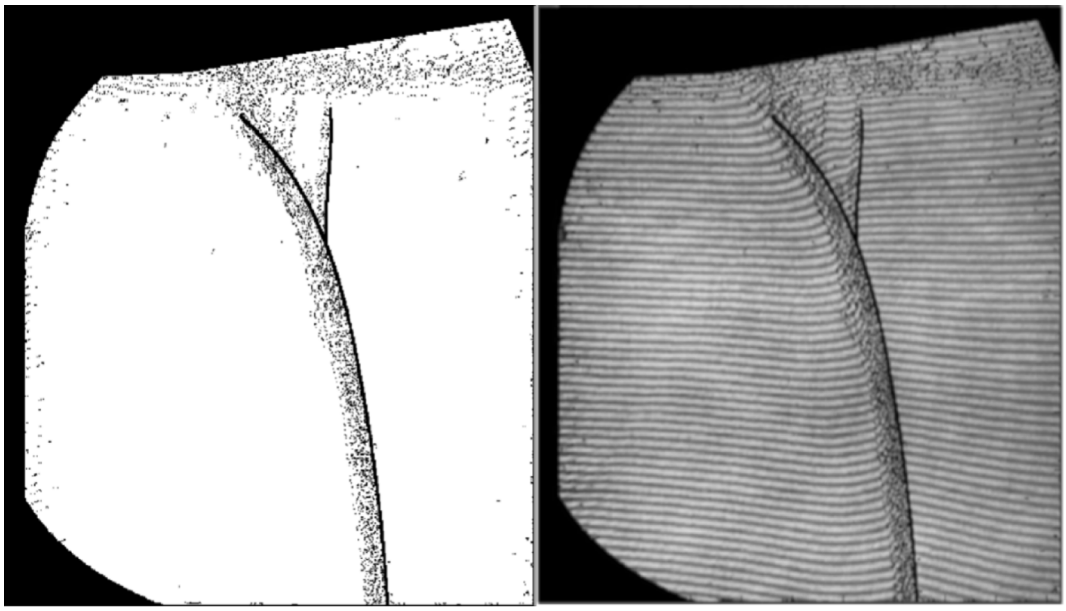

Fig. 8. Complete mask (a) and its position in the flow field (b).

where

Authors of [20] calculate the error of normalized density as:

$$\frac{\delta n \approx \lambda \bullet p_s . T_{ref}}{d \bullet T_s . p_{ref} . \delta_{flow} . \frac{\delta\phi}{\phi}}$$

that is valid if ideal light source monochromaticity is assumed. We decided to research the applicability of this assumption for our case (The laser is a ClassIIIA, Transverse Industries Co., Ltd device.).

In order to calculate the error introduced by λ, the spectrum of laser source has been measured using an SR-303i monochromator and ICCD iSTAR DH740 spectroscopic camera. The actual spectrum of the laser is depicted in Fig. 10.

To compare the significance of the two abovementioned sources of error, we transform equation (5) into a form clearly indicating variables and (constant) parameters:

$$\gamma = A \bullet \phi . \lambda$$

where:

$$\begin{cases} A & = \frac{\rho_s}{2.\pi.\mathrm{d}.\delta} & = const \\ \phi & = \phi_{ref} - \phi_{flow} & \\ \gamma & = \rho_{ref} - \phi\rho_{flow} & \end{cases}$$

The resultant uncertainty is influenced by uncertainties of two values: ϕ and λ. Calculating the relative uncertainty of γ we obtain:

$$\frac{d\gamma}{\gamma} = \frac{d\phi}{\phi} + \frac{d\lambda}{\lambda} \tag{6}$$

The relative error resulting from ϕ can be estimated as in [26] and [24] it is justified, that

$$\frac{d\phi}{\phi} \approx 0.02. \tag{7}$$

The relative error of λ can be estimated, for our measured spectrum of laser light source, to be:

$$\frac{d\lambda}{\lambda} \approx \frac{0.29}{646} = 0.04\% \tag{8}$$

The value of (8) is of two orders of magnitude smaller than the one from formula (7). Taking this together with Eq. (6) into account, it can be stated than the only significant error is caused by the uncertainty the calculation of φ. This proves the validity of assumption of [24] also for our case, with the conclusion of relative error of density not bigger than 0.5%.

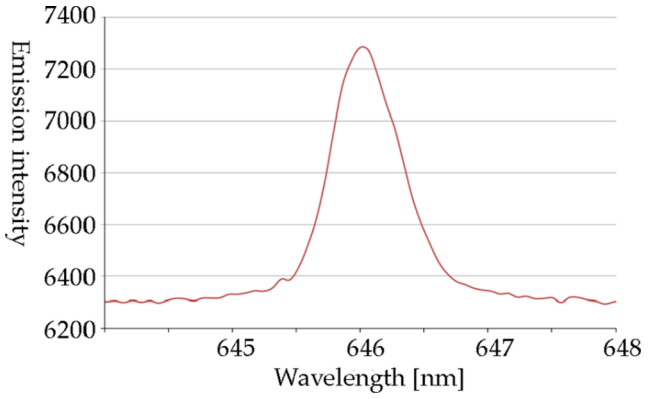

Fig. 10. Distribution of emission intensity of diode laser light source.

4. Results

Using two input interferograms (Fig. 1) as the input data for the programme, the resultant phase shift is depicted in Fig. 11.

The phase result can be easily converted to density field using a measured value in any single point of the region of investigation. At least a single measured value is necessary, as equation (5) defines a relation between the phase shift and the density change that it is accompanied by. There is no relation to the absolute value of density. The result is expressed in terms of difference between the reference density (corresponding to the no-flow image that we arbitrarily chose as reference conditions) and the flow of interest (the flow-on condition that we select as the one of interest). We have measured this reference value with a pressure scanner in the pressure taps in the nozzle (Fig. 3). This value substituted to Eq. (5) yields an absolute value of density, an 'origin value' for the phase shift map. Starting from that point, the value of density is unambigously related to an absolute value of density. This is called 'calibration' and it is valid for any flow that holds the value of pressure at the selected point. For our experiments, it is very often that in a point upstream of the shock wave (in the supersonic flow region) this value is constant and not influenced by the phenomena taking place in the shock wave region for a wide class of experiments. The ambient conditions were measured with barometer and thermometer outside of the nozzle (Fig. 2). In the cross sections of the obtained map the characteristic elements of the flow, including boundary layer and shock wave, are clearly visible (an exemplary calculated density map cross section is shown in Fig. 12).

The density distribution is marked with the solid black line. It was calculated along the line marked with dashed white line in Fig. 11. The dashed green and blue lines correspond to the position of the shock wave and they are also indicated in Fig. 11.

The magnitude of the density change (calculated with FTFA method) across the shockwave is marked in Fig. 12 with a thick blue, vertical arrow. As a coarse validation, this value has been also calculated using normal shock wave relations for the measured case of M = 1.34. The two values agree with precision of 2%. This proves, that using a more fine-tuned mask, a precise values of shock wave angle, and not an isentropic approximation one would obtain a fairly good precision of this

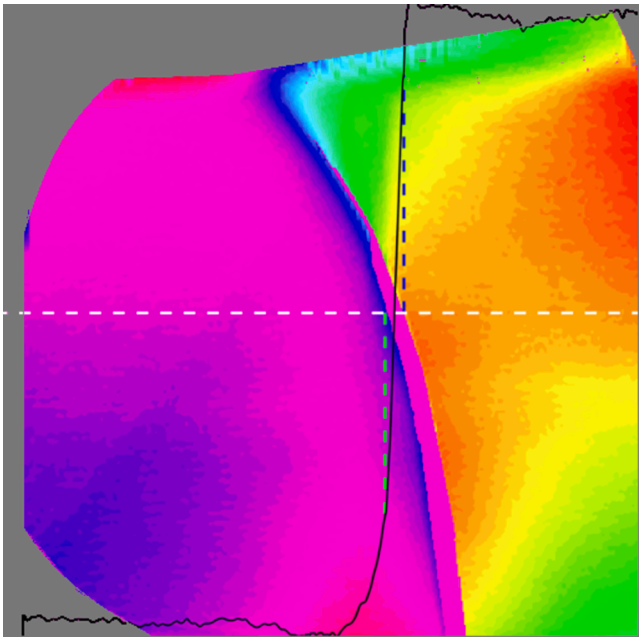

Fig. 11. Resultant phase shift map.

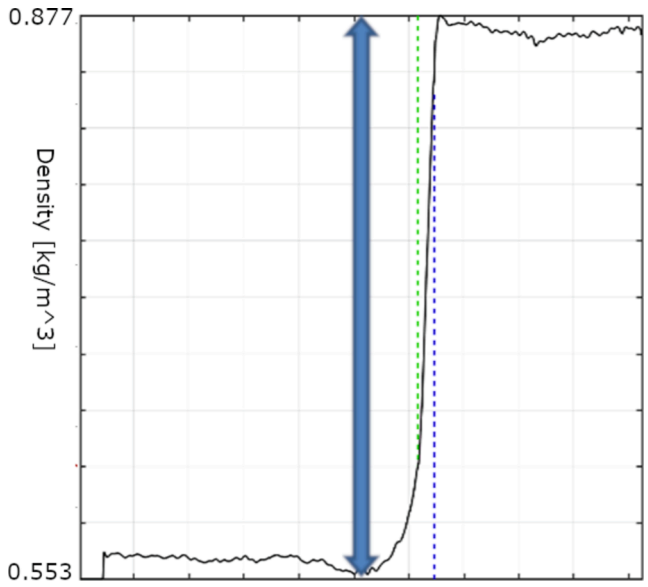

Fig. 12. Density distribution across a shock wave.

measurement method. The position of cross section can be selected freely, including regions of complex phenomena. For example, the results cover the region of triple point [27], which is still extremely difficult in terms of measurement.

5. Discussion and conclusions

The main aim of the FTFA is to use all the phase information that is contained in the interferogram. Using this method, the radiometric resolution of the final results increases significantly because they originate from at least 8-bit values instead of a single bit. The resolution in terms of gas parameters and space can be easily and significantly improved simply by the use of a better recording technique.

Moreover, in the past the only method that could use less good optics was holographic interferometry [6]. The reason for that is that it allows for the creation of interference patterns from images without flow and with flow thus showing fringes caused by changes between the two and ignoring fringes due to optical defects. We describe a method to achieve the same without the complexity of a holographic system. It is based on calculating the phase shift that is introduced to the interferogram by the flow. Once this shift is calculated by the means of FFT, it can be transformed into density using a simple algebraic transformation taking into account the parametres of the experiment.

The presented approach allows one to obtain a very good quality maps of parameters in planar nozzle without the complexity of holographic technique. Such results are still valuable and very demanded. The required numerical steps are easy to follow nowadays even with a desktop computer. The very high applicability for complex SWBLI flows has been emphasized in this paper due to the field of interest of the authors, but the method is not restricted to this field.

Declaration of Competing Interest

The authors declare that they have no known competing financial interests or personal relationships that could have appeared to influence the work reported in this paper.

References

[1] K.P. Zetie, How does a Mach-Zehnder interferometer work, Phys. Educ. 35, 46.
[2] A.J. Smits, Flow Visualization: Techniques and Examples, 2rd ed., Imperial College Press, 2012.
[3] Initial Adjustment of the Mach-Zehnder interferometer. The Review of Scientific instruments, **1953**, vol. 23, 4.
[4] J. Telega, R. Szwaba, P. Doerffer, Shock waves asymmetry in a symmetric nozzle, Symmetry 11 (2019) 1477, https://doi.org/10.3390/sym11121477.
[5] M. Takeda, H. Ina, S. Kobayashi, Fourier-transform method of fringe-pattern analysis for computer-based topography and interferometry, J. Opt. Soc. Am 72 (1) (1982) 156, https://doi.org/10.1364/JOSA.72.000156.
[6] R. Bracewell, The Fourier Transform & Its Applications, 3rd ed.; McGraw-Hill: New York, USA, 1965.
[7] D.W. Robinson, G.T. Reid, Eds., Interferogram Analysis: Digital Fringe Pattern Measurement Techniques, Institute of Physics, Bristol, England, 1993.
[8] M. Takeda, Fourier fringe analysis and its application to metrology of extreme physical phenomena: a review [invited], Appl. Opt. 52 (2013) 20–29.
[9] J. Li, X.R. Su, L.R. Guo, Improved Fourier transform profilometry for the automatic measurement of three-dimensional object shapes, Opt. Eng. 29 (1993) 1439–1444.
[10] F. Berryman, P. Pynsent, J. Cubillo, The effect of windowing in fourier transform profilometry applied to noisy images, Opt. Lasers Eng. 41 (6) (2004) 815–825.
[11] D.R. Burton, M.J. Lalor, Multichannel Fourier fringe analysis as an aid to automatic phase unwrapping, Appl. Opt. 33 (14) (1994) 2939, https://doi.org/10.1364/AO.33.002939.
[12] X. Su, W. Chen, Fourier transform profilometry: a review, Opt. Lasers Eng. 35 (5) (2001) 263–284.
[13] Shijie Feng, Qian Chen, Guohua Gu, Tianyang Tao, Liang Zhang, Yan Hu, Wei Yin, Chao Zuo, Fringe pattern analysis using deep learning, 2019, Adv. Photon. 1(2) 025001 doi.org/10.1117/1.AP.1.2.025001.
[14] N. Fomin, E. Lavinskaya, P. Doerffer, J. Szumski, R. Szwaba, J. Telega, Quantitative diagnostics of shock wave - boundary layer interaction by digital speckle photography. In: Proceedings{10.1007/978-3-540-85168-4_73, 1st ed.; Hannemann, K., Seiler, F., Springer Berlin Heidelberg: Berlin, Heidelberg, Germany, 2009, Volume 3, pp. 457–462.
[15] K.B. Itoh, Analysis of the phase unwrapping problem, Appl. Opt. 1982, 21, pp. 2470.
[16] D.J. Bone, Fourier fringe analysis–the two-dimensional phase unwrapping problem, Appl. Opt. 30 (25) (1991) 3627, https://doi.org/10.1364/AO.30.003627.
[17] G.S. Settles, M.J. Hargather, A review of recent developments in schlieren and shadowgraph techniques, Measur. Sci. Technol. 28 (4) (2017) 042001, https://doi.org/10.1088/1361-6501/aa5748.
[18] I.G. Priest, A simplified formula for the change in order of interference due to changes in temperature and pressure of air, Bull. Bureau Standards, 9.
[19] S.A. Coronel, J. Melguizo-Gavilanes, S. Jones, J.E. Shepherd, Temperature field measurements of thermal boundary layer and wake of moving hot spheres using interferometry, Exp. Thermal Fluid Sci. 90 (2018) 76–83, https://doi.org/10.1016/j.expthermflusci.2017.08.031.
[20] A. Coschignano, H. Babinsky, Normal shock wave-turbulent boundary layer interactions in transonic intakes at incidence, 2018 AIAA Aerospace Sciences Meeting 2018, https://doi.org/10.2514/6.2018-1513.
[21] P. Doerffer, J. Telega, Flow control effect on unsteadiness of shock wave induced separation, J. Therm. Sci. 22 (6) (2013) 511–516.
[22] P. Flaszynski, R. Szwaba, Experimental and numerical analysis of a streamwise vortex generator for subsonic flow, Chem. Process Eng. 27 (3) (2006) 985–997.
[23] F. Wasilczuk, P. Flaszynski, P. Kaczynski, R. Szwaba, P. Doerffer, K. Marugi, Leakage flow analysis in the gas turbine shroud gap, Aircraft Eng. Aerospace Technol. 91 (8) (2019) 1077–1085, https://doi.org/10.1108/AEAT-01-2018-0038.
[24] H. Liepmann, A. Roshko, Elements of Gas Dynamics, 1st ed., John Wiley and Sons, New York, USA, 1957.
[25] A.F.P. Houwing, K. Takayama, Z. Jiang, M. Sun, K. Yada, H. Mitobe, Interferometric measurement of density in nonstationary shock wave reflection flow and comparison with CFD, Shock Waves 14 (1-2) (2005) 11–19.
[26] K. Takayama, Application of holographic interferometry to shock wave research, Proc. SPIE (1983) 174–180.
[27] R. Szwaba, P. Doerffer, K. Namieśnik, O. Szulc, Flow structure in the region of three shock wave interaction, Aerospace Sci. Technol. 8 (6) (2004) 499–508.